# Four degree-of-freedom lumped parameter model of the foot-ankle system exposed to vertical vibration from 10 to 60 Hz with varying centre of pressure conditions

Katie A. Goggins[a,b], Delphine Chadefaux[c,d], Marco Tarabini[d], Marc Arsenault[a], W. Brent Lievers[a,b] and Tammy Eger[b,e]

[a]Bharti School of Engineering, Laurentian University, Sudbury, Canada; [b]Centre for Research in Occupational Safety and Health, Laurentian University, Sudbury, Canada; [c]Insitut de Biomecanique Humaine Georges Charpak, Université Paris 13 Nord, Villetaneuse, France; [d]Department of Mechanics, Politecnico di Milano, Lecco, Italy; [e]School of Human Kinetics, Laurentian University, Sudbury, Canada

**ABSTRACT**

Modelling the foot-ankle system (FAS) while exposed to foot-transmitted vibration (FTV) is essential for designing inhibition methods to prevent the effects of vibration-induced white-foot. K-means analysis was conducted on a data set containing vibration transmissibility from the floor to 24 anatomical locations on the right foot of 21 participants. The K-means analysis found three locations to be sufficient for summarising the FTV response. A three segment, four degrees-of-freedom lumped parameter model of the FAS was designed to model the transmissibility response at three locations when exposed to vertical vibration from 10 to 60 Hz. Reasonable results were found at the ankle, midfoot, and toes in the natural standing position (mean-squared error ($\varepsilon$) = 0.471, 0.089, 0.047) and forward centre of pressure (COP) ($\varepsilon$ = 0.539, 0.058, 0.057). However, when the COP is backward, the model does not sufficiently capture the transmissibility response at the ankle ($\varepsilon$ = 1.09, 0.219, 0.039).

**Practitioner summary** The vibration transmissibility response of the foot-ankle system (FAS) was modelled with varying centre of pressure (COP) locations. Modelling the FAS using three transmissibility locations and two foot segments (rearfoot and forefoot) demonstrated reasonable results in a natural standing and forward COP position to test future intervention strategies.

**Abbreviations:** COP: centre of pressure; DOF: degrees-of-freedom; FAS: foot-ankle system; FTV: foot-transmitted vibration; HAVS: hand-arm vibration syndrome; LDV: laser Doppler vibrometer; LP: lumped-parameter; VWT: vibration-induced white-toes; WBV: whole-body vibration

**KEYWORDS**

Foot-ankle vibration model; foot-transmitted vibration; vibration-induced injury; standing vibration

## 1. Introduction

Prolonged exposure to occupational foot-transmitted vibration (FTV) can cause neurological, vascular, and osteoarticular symptoms in the feet (House et al. 2011; Thompson et al. 2010). Workers are exposed to FTV when standing on a vibrating surface or platform (Eger et al. 2014) in industries such as construction (House et al. 2011), forestry (Jack and Oliver 2008), welding (Toibana et al. 1994), rock drilling (Hasiguichi et al. 1994) and underground mining (Leduc et al. 2011; Hedlund 1989). Moreover, heavy equipment operated by foot pedals also exposes the workers to FTV (Tingsgard and Rasmussen 1994), leading to an increased risk of developing vibration-induced white-toes (VWT). Symptoms of VWT parallel those of vibration-induced white-finger – the vascular component of hand-arm vibration syndrome (HAVS) – where damage to the blood vessels can cause constriction and result in episodic blanching of the digits due to reduced blood flow (Schweigert 2002). Ultimately, prolonged occupational exposure to FTV can lead to worker disability with chronic tingling, numbness, and pain in the feet (Eger et al. 2014).

The ability to quantify the extent of disability caused by FTV is confounded by the fact that it has been historically grouped with whole-body vibration (WBV) exposure (e.g. standing WBV in International

CONTACT Katie Goggins kx_goggins@laurentian.ca Centre for Research in Occupational Safety and Health, 935 Ramsey Lake Road, Sudbury, ON, Canada

Standards (ISO-2631-11 1997)). A further consequence of this lack of attention is that modelling of FTV has been virtually ignored relative to the number of lumped-parameter (LP) models that have been developed to predict the biological response to both WBV (Coermann 1962; Smith and Kazarian 1994; Zhou and Griffin 2014) and hand-transmitted vibration exposure (Reynolds and Soedel 1972; Mishoe and Suggs 1977; Wood, Suggs, and Abrams 1978; Gurram, Rakheja, and Gouw 1995; Dong et al. 2007). Whole-body vibration LP models usually simulate a standing human body and account for the effects of vertical vibration (*z*-axis) exposure on the human body as whole, but they do not typically include the foot (or parts thereof) as distinct components (Zadpoor and Nikooyan 2010; Subashi, Matsumoto, and Griffin 2008; Gupta and Gupta 2017). Therefore, existing WBV models are incapable of capturing foot-specific behaviour that can result in VWT.

Only two LP models with detailed foot representation have been developed to model vibration response. The five-mass LP model of Wee (2012) was validated over a frequency range of 10–50 Hz at 5 Hz increments using transmissibility data collected at the medial malleolus and tibial tuberosity. No data was collected on the foot itself. Moreover, the test subjects were seated rather than standing, with various loads placed on their knees. Neither the model nor the validation data is suitable for standing workers. A six mass model (four foot and two body segments) has also been presented which captures the vibration response of the foot over 10–100 Hz in a neutral standing position (Chadefaux et al. 2020). Although this model incorporated more details of the foot, it was based on the person remaining in a neutral position and did not incorporate the influence of changes in the centre of pressure.

Recently, it has been discovered that the average resonant frequencies of the different regions of the foot (i.e. toes, midfoot, hindfoot) vary based on the centre of pressure (Goggins et al. 2019b). In other words, as someone shifts their weight to their forefoot, the resonant frequencies of the toes increase. The opposite is also true: concentrating the COP towards the hindfoot causes an increase in resonant frequency at the ankle (Goggins et al. 2019b). Since the overall body posture will have an effect on the response of the foot, the long-term objective of vibration modelling would be the development of a full-body model that can simultaneously capture the FTV and WBV responses. The increasing complexity associated with these models means that efforts must be made to reduce the number of components within different regions of the model (e.g. trunk, lower limbs, feet) to ensure the total model is tractable.

A recent analysis of the foot-ankle system's (FAS) transmissibility suggests that the overall response can be represented with measurements taken at four anatomical locations (nail bed of first toe, distal head of first metatarsal, middle of second metatarsal, and the lateral malleolous) (Goggins et al. 2020). Chadefaux et al. (2020) developed a model with four foot segments and five transmissibility responses. Further simplification may be possible; however, a foot that is composed of two segments is potentially the simplest model that would allow for different regions responses of the toes, midfoot, and hindfoot (Goggins et al. 2019a). It would also be the simplest that incorporates important anatomic features that are expected to contribute to the overall behaviour (Dawe and Davis 2011): the medial longitudinal arch of the foot (Simkin and Leichter 1990; Salathe, Arangio, and Salathe 1986) and the plantar fascia (Gefen 2003; Kim and Voloshin 1995).

The goal of the current work is to assess whether a three-segment mode (two foot segments, one body segment) is capable of predicting the frequency response of the foot and ankle under three scenarios: neutral, forward, and backwards COP. K-means analysis of the experimental data was performed to identify the number of regions and measurement points that would be representative of the response for all three COP values. The model structure based on the K-means analysis was then created and the equations for that model were determined. Finally, the model was fit to previously collected human biodynamic response data. Identifying the simplest model of the foot capable of predicting its biomechanical response to vibration will enable incorporation into more holistic WBV simulation efforts, and will reduce the number of experimental measurement points needed to validate such models. It is hoped that improved predictive abilities can one day be used for interventions to reduce the incidence and severity of VWT.

## 2. Methodology

The model was created using a vertical vibration transmissibility data-set, from 10 to 200 Hz, that includes measurements at 24 anatomical locations of the foot, under three loading conditions, from 21 participants (Goggins et al. 2019a, 2019b) (Figure 1). One challenge when developing an LP model is determining how many segments to include. Previous analysis of this

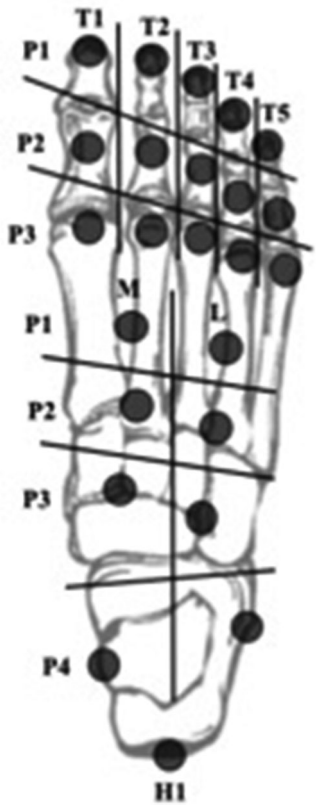


Figure 1. Twenty-four anatomical locations where transmissibility measurements were taken (Goggins et al. 2019a, 2019b).

data, based on the transmissibility magnitude, found four locations (nail bed of first phalange; distal head of first metatarsal; proximal head of second metatarsal; lateral malleolus) were sufficient to capture the FTV response (Goggins et al. 2020). In this work, a modified K-means clustering analysis was performed to provide guidance about which unique anatomical regions should be represented in the foot model and which measurement points are representative of those regions.

## 2.1. K-means analysis: identify anatomic regions

### 2.1.1. Algorithm

K-means clustering is typically performed to minimise the total variance (MacQueen 1965), $\sigma^2$, that is, the sum of the variance in each group, $\sigma_g^2$. One curve, $T(f)$, the average transmissibility response over the frequencies, $f$, from 10–200 Hz, was taken as representative of the behaviour at each of the 24 locations. The variance of a group, $\sigma_g^2$, was then calculated as the sum of the variances of the individual curves, $T_i(f)$, relative to the group average, $\overline{T}(f)$.

Since the intent was to identify regions of the foot having comparable responses, an additional spatial constraint was added. A connectivity network was superimposed on the measurement points that described their positions relative to one another. Groups were constrained to be connected so as to ensure, for example, that the big toe and the heel were not found to be part of the same 'regional' group.

The pseudo-code for the K-means clustering algorithm with superimposed regional constraints is as follows, assuming an initial grouping for each point:

1. Calculate the averages and variance for each group;
2. Calculate the total variance;
3. Identify the 'edge points', the measurement points adjacent to another group;
4. Sort the edge points, based on their individual variance from the group average, largest to smallest;
5. Go through each edge point and attempt to switch it to each adjacent group;
6. Calculate the updated total variance;
7. Keep a switch if it reduces the total variance and maintains group connectivity, otherwise revert it and try the next edge point in 5;
8. If an edge point switches group, return to step 1, otherwise a local minimum has been found.

A common issue with K-means clustering techniques is that they can only guarantee a local, and not a global, minimum. Therefore, for each clustering attempt, 100 random initial groups were assigned using an initial seeding and region growing approach that ensured group connectivity. The clustering algorithm was then applied. The result with the lowest total variance was identified as the final solution.

One further simplification was made. Nine measurement points were excluded (white circles in Figure 2) based on their difficulty to measure with a laser Doppler vibrometer (LDV) or accelerometer. The excluded points included all measures on the fourth and fifth toes (T4 and T5 in Figure 1) due to a very small surface area for measurement, and two measurement locations on the midfoot and one on the heel which can be influenced by skin artefact from ligament contracture.

### 2.1.2. K-means analysis: findings

Using the algorithm described above, clustering of the transmissibility responses was performed separately for the forward, natural, and backward data published previously (Goggins et al. 2019a, 2019b). The minimum variance findings are presented with the COP in the forward (Figure 2), natural (Figure 3),

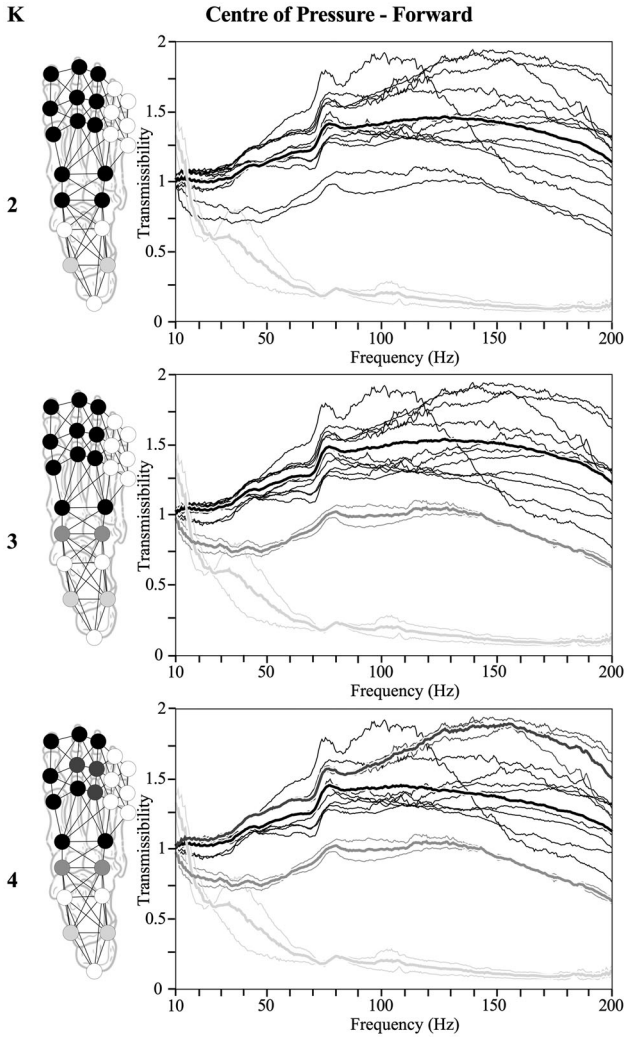


Figure 2. Total variance results from K-Means cluster analysis conducted on transmissibility results with the centre of pressure in the forward position (Goggins et al. 2019b). White circles are excluded locations. Thin transmissibility lines are experimental measurements, and the corresponding thick transmissibility line is the average of the group of locations.

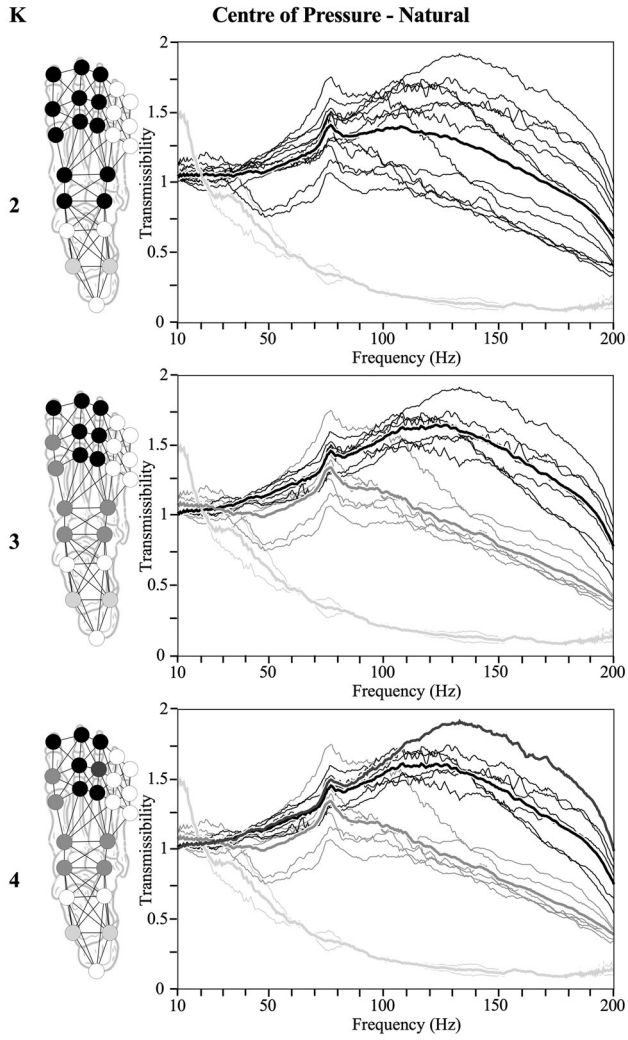


Figure 3. Total variance results from K-means cluster analysis conducted on transmissibility results with the centre of pressure in the natural position (Goggins et al. 2019a). White circles are excluded locations. Thin transmissibility lines are experimental measurements, and the corresponding thick transmissibility line is the average of the group of locations.

and backward (Figure 4) positions for two, three, and four solution groups.

Results of the modified K-means cluster analysis suggest that three groups (toes, midfoot, ankle) provide the most consistent results. While increasing the number of groups does decrease the total variance, at $K = 4$, isolated clusters begin to appear, where only a single anatomical location represents a group. Any of the measurement points within these three groups could be taken as representative of that region; however, certain anatomic locations are easier to landmark and measure with an accelerometer or LDV (Goggins et al. 2020). Therefore, the nail of the big toe (T1P1), the third metatarsal (L2), and the lateral malleolus (L4) are recommended and will be used in subsequent analyses as the reference functions.

### 2.2. Description of the proposed LP model

Based on the results of the K-means analysis, a planar LP model was devised to incorporate three transmissibility responses – at the ankle, midfoot and toes – as the reference functions with the objective of replicating the dynamic behaviour of a FAS supporting half of the total human body mass (Figure 5). The medial longitudinal arch, consisting of the calcaneus, talus, navicular, three cuneiforms, and the heads of the first three metatarsals, is simplified into a truss structure (Gefen 2003; Kim and Voloshin 1995). As such the LP

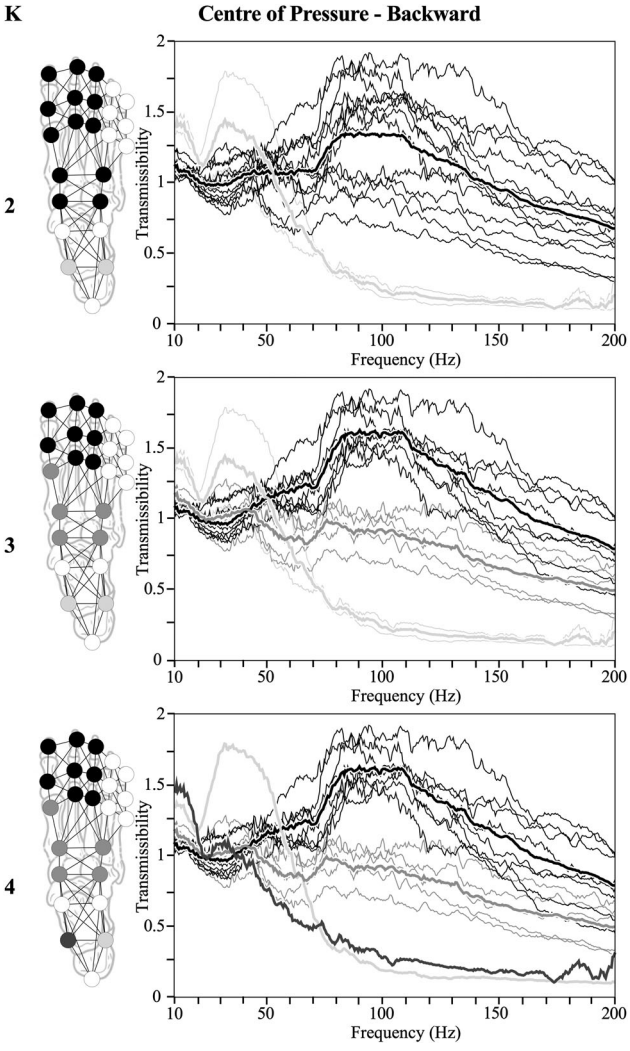


Figure 4. Total variance results from K-Means cluster analysis conducted on transmissibility results with the centre of pressure in the backward position (Goggins et al. 2019b). White circles are excluded locations. Thin transmissibility lines are experimental measurements, and the corresponding thick transmissibility line is the average of the group of locations.

model includes two rigid body segments connecting nodes $P_1$ and $P_3$ (rearfoot) and nodes $P_2$ and $P_3$ (forefoot). The mass, length and mass moment of inertia (about its centre of mass $Q_i$) of the $i$ th segment ($i$= 1, 2) are denoted as $m_i$, $l_i$ and $J_i$, respectively. The inertial properties of the rearfoot ($i_1$) and forefoot segments ($i_2$) used in the planar LP FAS model were: 147 g, 79.3 mm, 280 kg·mm$^2$, and 343 g, 106 mm, 5.554 kg·mm$^2$, respectively (Isman and Inman 1969; Aruin and Zatsiorsky 1984; Zatsiorsky 2002). Meanwhile, the half human body supported by the FAS is represented by a rigid body whose mass $m_3$ = 35 kg was identified experimentally based on data obtained from 21 participants exposed to standing FTV (Goggins et al. 2019a, 2019b). The midfoot, for its part, is represented by a rigid body of negligible mass where the rearfoot and forefoot segments are connected by a passive revolute joint (node $P_3$).

The fat pads at each of the support locations were assumed to be viscoelastic materials based on a Kelvin–Voigt model with stiffness $k_i$, rest length $\delta_i$ and damping $c_i$ ($i$ = 1, 2). The plantar aponeurosis, for its part, is represented by a spring-damper system of stiffness $k_3$, rest length $\delta_3$ and damping $c_3$ connecting the calcaneus and metatarsophalangeal articulation (Wee 2012; Kim and Voloshin 1995). Finally, the connection between the midfoot and body is modelled as having stiffness $k_4$, rest length $\delta_4$ and damping $c_4$.

Referring to Figure 5, the midfoot and body are constrained to translate along the $Y$ axis of a fixed $XY$ reference frame. A harmonic displacement $y_{in}(t)$ of the plate on which the foot is resting is provided as the input to the model. The fat pads at each of the foot support locations are assumed to be able to slide freely along the plate. The model thus has a total of four degrees-of-freedom (DOF). The coordinates used to represent the motion of the FAS includes angles $\theta_1$ and $\theta_2$ measured form the vertical to the rearfoot and forefoot segments, respectively, along with the heights of the midfoot ($y_1$) and body ($y_2$) measured with respect to the plate.

### 2.3. Dynamic modelling of the LP model

The dynamic model of the LP model is developed here using the Lagrangian formulation (Ji, Zhou, and Zhang 2013), i.e.,

$$\frac{d}{dt}\left(\frac{\partial T}{\partial \dot{\boldsymbol{x}}}\right) - \frac{\partial T}{\partial \boldsymbol{x}} + \frac{\partial D}{\partial \dot{\boldsymbol{x}}} + \frac{\partial U}{\partial \boldsymbol{x}} = 0, \tag{1}$$

where $T$, $D$, and $U$ are the system's kinetic energy, dissipation function and potential energy, respectively, while $x = [y_1, y_2, \theta_1, \theta_2]^T$ is the vector of generalised coordinates used to represent its motion. The positions of points $P_1$, $P_2$, and $P_3$ in Figure 5 are obtained as

$$\boldsymbol{p}_1 = \boldsymbol{p}_3 - \ell_1 \begin{bmatrix} \sin\theta_1 \\ \cos\theta_1 \end{bmatrix}, \quad \boldsymbol{p}_2 = \boldsymbol{p}_3 - \ell_2 \begin{bmatrix} -\sin\theta_2 \\ \cos\theta_2 \end{bmatrix}, \quad \boldsymbol{p}_3 = \begin{bmatrix} 0 \\ y_1 + y_{in}(t) \end{bmatrix}, \tag{2}$$

whereas the lower extremities of the two fat pads correspond to points $P_1'$ and $P_2'$ of positions

$$\boldsymbol{p}_1'' = \begin{bmatrix} -\ell_1 \sin\theta_1 \\ y_{in}(t) \end{bmatrix}, \quad \boldsymbol{p}_2' = \begin{bmatrix} \ell_2 \sin\theta_2 \\ y_{in}(t) \end{bmatrix}. \tag{3}$$

Meanwhile, the locations of the centres of mass of the rearfoot and forefoot links as well as the half human body are

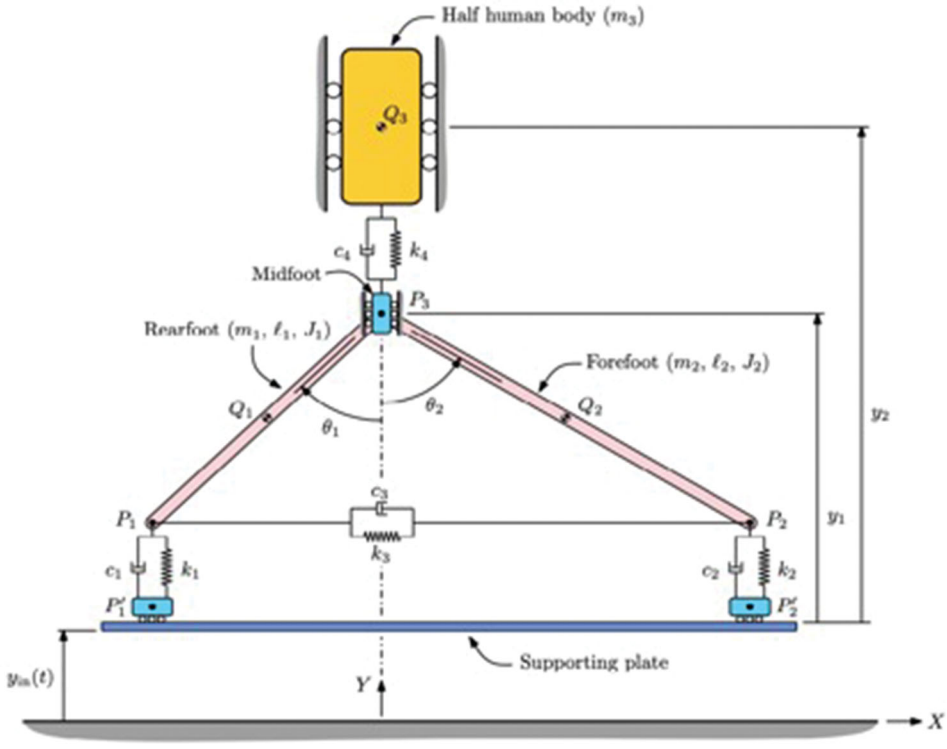


Figure 5. Schematic representation of the proposed planar LP model of the FAS.

$$\boldsymbol{q}_1 = \boldsymbol{p}_3 - \frac{\ell_1}{2}\begin{bmatrix}\sin\theta_1\\ \cos\theta_1\end{bmatrix},$$
$$\boldsymbol{q}_2 = \boldsymbol{p}_3 - \frac{\ell_2}{2}\begin{bmatrix}-\sin\theta_2\\ \cos\theta_2\end{bmatrix}, \quad (4)$$
$$\boldsymbol{q}_3 = \begin{bmatrix}0\\ y_2 + y_{in}(t)\end{bmatrix}$$

The system's kinetic energy, dissipation function and potential energy may thus be expressed as

$$T = \frac{1}{2}\sum_{i=1}^{3}\left(m_i\dot{\boldsymbol{q}}_i^T\dot{\boldsymbol{q}}_i\right) + \frac{1}{2}\sum_{i-1}^{2}\left(J_i\dot{\theta}_i^2\right) \quad (5)$$

$$D = \frac{1}{2}\sum_{i=1}^{2}c_i\|\dot{\boldsymbol{p}}_i - \dot{\boldsymbol{p}}_i'\|^2 + \frac{1}{2}c_3\|\dot{\boldsymbol{p}}_2 - \dot{\boldsymbol{p}}_1\|^2 + \frac{1}{2}c_4\|\dot{\boldsymbol{q}}_3 - \dot{\boldsymbol{p}}_3\|^2 \quad (6)$$

$$U = \sum_{i=1}^{3}m_i g\boldsymbol{j}\cdot\boldsymbol{q}_i + \frac{1}{2}\sum_{i=1}^{2}k_i\left(\|\boldsymbol{p}_i - \boldsymbol{p}_i'\| - \delta_i\right)^2 + \frac{1}{2}k_3\left(\|\boldsymbol{p}_2 - \boldsymbol{p}_1\| - \delta_3\right)^2 + \frac{1}{2}k_4\left(\|\boldsymbol{q}_3 - \boldsymbol{p}_3\| - \delta_4\right)^2 \quad (7)$$

respectively, where $g = 9.81\ \mathrm{m/s^2}$ and $\boldsymbol{j} = [0, 1]^T$.

Given the demonstrated limited impact of nonlinear effects in the biodynamic response of standing participants (Tarabini et al. 2014), the dynamic model is linearised about the system's static equilibrium configuration which corresponds to $\overline{\boldsymbol{x}} = [\overline{y}_1, \overline{y}_2, \overline{\theta}_1, \overline{\theta}_2]^T$. The required rest lengths of the springs to ensure static equilibrium in this configuration (i.e. $\delta_i$ with $i = 1, 2, 3, 4$) may be found in terms of $\overline{\boldsymbol{x}}$ from the solution of the static equilibrium equations, i.e.,

$$\frac{\partial U}{\partial \boldsymbol{x}}|_{x=\overline{x}} = 0 \quad (8)$$

The linearised dynamic model is finally obtained in the form

$$\boldsymbol{M}\Delta\ddot{x} + \boldsymbol{B}\Delta\dot{x} + \boldsymbol{K}\Delta x = -M_{in}\ddot{y}_{in}(t) \quad (9)$$

where $\Delta\boldsymbol{x} = \boldsymbol{x} - \overline{\boldsymbol{x}}$.

### 2.4. Vibration transmissibility

Expressions for the amplitude ratios of the output coordinates with respect to the input amplitude were developed:

$$\frac{\Delta Y_1}{Y_{in}} = f_1(\omega),\ \frac{\Delta Y_2}{Y_{in}} = f_2(\omega),\ \frac{\Delta\theta_1}{Y_{in}} = f_3(\omega),\ \frac{\Delta\theta_2}{Y_{in}} = f_4(\omega) \quad (10)$$

where $\omega$ is the input frequency (i.e. $y_{in}(t) = Y_{in}\sin(\omega t)$) while $Y_1$, $Y_2$, $\theta_1$ and $\theta_2$ are the amplitudes of the corresponding harmonic responses of the output coordinates (in steady state). Finally, $f_i(\omega)$ ($i = 1, 2, 3, 4$) represents some function of the input frequency (to be determined). It should also be noted that the

above amplitude ratios apply to deviations of the output coordinates from their nominal values (about which the model was linearised).

The system's frequency transfer functions from Equation (9) were obtained as follows:

$$\frac{\Delta \boldsymbol{X}(j\omega)}{Y_{in}(j\omega)} = [\boldsymbol{D}(j\omega)]^{-1}\boldsymbol{M}_{in}\omega^2 \tag{11}$$

where

$$\boldsymbol{D}(j\omega) = (\boldsymbol{K} - \omega^2\boldsymbol{M}) + j(\omega\boldsymbol{B}) \tag{12}$$

and

$$\frac{\Delta \boldsymbol{X}(j\omega)}{Y_{in}(j\omega)} = \left[\frac{\Delta Y_1(j\omega)}{Y_{in}(j\omega)}, \frac{\Delta Y_2(j\omega)}{Y_{in}(j\omega)}, \frac{\Delta \theta_1(j\omega)}{Y_{in}(j\omega)}, \frac{\Delta \theta_2(j\omega)}{Y_{in}(j\omega)}\right]^T \tag{13}$$

from which the desired amplitude ratios (as functions of the input frequency) with corresponding experimental data (Goggins et al. 2019a, 2019b) were obtained as:

$$\begin{aligned} \frac{\Delta Y_1}{Y_{in}} &= \left|\frac{\Delta Y_1(j\omega)}{Y_{in}(j\omega)}\right|, \quad \frac{\Delta Y_2}{Y_{in}} = \left|\frac{\Delta Y_2(j\omega)}{Y_{in}(j\omega)}\right|, \\ \frac{\Delta \theta_1}{Y_{in}} &= \left|\frac{\Delta \theta_1(j\omega)}{Y_{in}(j\omega)}\right|, \quad \frac{\Delta \theta_2}{Y_{in}} = \left|\frac{\Delta \theta_2(j\omega)}{Y_{in}(j\omega)}\right| \end{aligned} \tag{14}$$

where $|\cdot|$ represent the magnitude of the imaginary function corresponding to the argument.

### 2.5. Parameter estimation and optimisation

Initial values for each spring were set to $1 \times 10^4$ N/m and set to be in the range of 100 N/m and $5 \times 10^5$ N/m. Similarly, damping coefficients were initially guessed to be 10 Ns/m and set to be within the range of 0.1 Ns/m and $5 \times 10^3$ Ns/m. To optimise the model parameters ($k_{1\ldots4}$ and $c_{1\ldots4}$), a nonlinear curve-fitting in least-squares sense was used (lsqcurvefit function implemented in Matlab R2018a software). Then the deviation between the modelled and measured transmissibility (Equation (15)) and phase (Equation (16)) responses at the three locations (reconstructed quadratic error) ($\mathcal{E}$) was calculated as (Dong et al. 2008):

$$\mathcal{E}(T)_{1\ldots3} = \sqrt{\frac{1}{N}\sum_{f=10}^{60}\left|T\sim_{1\ldots3}(f) - T_{1\ldots3}(f)\right|^2} \tag{15}$$

$$\mathcal{E}(P)_{1\ldots3} = \sqrt{\frac{1}{N}\sum_{f=10}^{60}\left|P\sim_{1\ldots3}(f) - P_{1\ldots3}(f)\right|^2} \tag{16}$$

where $f$ is the frequency, $T\sim_{1\ldots3}$ and $T_{1\ldots3}$ are the modelled and measured transmissibility functions, $P\sim_{1\ldots3}$ and $P_{1\ldots3}$ are the modelled and measured phase functions, and $N$ is the length of the discrete transmissibility functions. The optimisation was run on the transmissibility and phase functions to a maximum of $1 \times 10^4$ iterations and stopped once residual deviations were below $1 \times 10^{-10}$. After trials using the entire frequency range of the reference functions (10–200 Hz), it became evident that the frequency range need to be limited. As such, a frequency range from 10 to 60 Hz was used to incorporate the frequencies at which equipment operators could be exposed to FTV (Eger et al. 2014).

### 2.6. Sensitivity analysis

Finally, to estimate the model sensitivity a Monte Carlo analysis (Chadefaux et al. 2020) was conducted using 100 randomised combinations of the stiffness and damping parameters to estimate the three transmissibility functions. The stiffness and damping parameters were varied based on an assumed normal distribution with a mean equivalent to its optimised value and a standard deviation of 20% of the mean. The variability between the optimised transmissibility function and the Monte Carlo simulated transmissibility functions were estimated with the percentage of deviation between the two values at 10 Hz intervals.

## 3. Results

The estimated parameters of the 4-DOF lumped parameter model of the FAS (Figure 5) exposed to vertical vibration between 10 and 60 Hz are presented in Table 1. Separate sets of parameters are given for each of the three COP positions (forward lean, neutral, backward lean) studied in the experiments.

The stiffness of the plantar aponeurosis $(k_1)$ was the greatest in the natural standing position and the least when the COP was closer to the heel, while the damping $(c_1)$ remained at the minimum (0.1 Ns/m) regardless of the COP location. The stiffness of the mass of the human body $(k_3)$ was the largest in the natural standing position, and was the imposed minimum (100 N/m) in the forward and backward COP locations. The damping of the mass of the body $(c_3)$ is the largest in the natural position, followed by the forward and then backward COP locations.

The stiffness of the calcaneus fat pad $(k_2)$ is the greatest in the natural standing position, and the lowest in the backward COP position; the damping of the calcaneus $(c_2)$ is the greatest in the forward COP position, and the imposed minimum (0.1 Ns/m) in the natural and forward COP positions. Finally, the stiffness

Table 1. Estimated model parameters, using single location transmissibility responses T1P1, L2, L4), including the stiffness and damping coefficients of each model segment in the natural standing position and under two changes in centre of pressure location (towards the forefoot and rearfoot).

| | | COP location | | | |
|---|---|---|---|---|---|
| Parameter | Unit | Forward | Natural | Backward | Description |
| $k_1$ | N/m | $1.33 \times 10^6$ | $2.86 \times 10^6$ | $4.11 \times 10^5$ | Stiffness of the plantar aponeurosis |
| $k_2$ | | $2.76 \times 10^5$ | $9.00 \times 10^5$ | $1.72 \times 10^5$ | Stiffness of the calcaneus fat pad |
| $k_3$ | | 100 | $1.21 \times 10^4$ | 100 | Stiffness of the mass of the body |
| $k_4$ | | $5.57 \times 10^5$ | $6.46 \times 10^4$ | 102 | Stiffness of the tarsals fat pad |
| $c_1$ | Ns/m | 0.10 | 0.10 | 0.10 | Damping of the plantar aponeurosis |
| $c_2$ | | $1.26 \times 10^4$ | 0.10 | 0.10 | Damping of the calcaneus fat pad |
| $c_3$ | | $2.24 \times 10^3$ | $5.09 \times 10^3$ | 621 | Damping of the mass of the body |
| $c_4$ | | 0.10 | $7.89 \times 10^3$ | $2.52 \times 10^5$ | Damping of the tarsals fat pad |

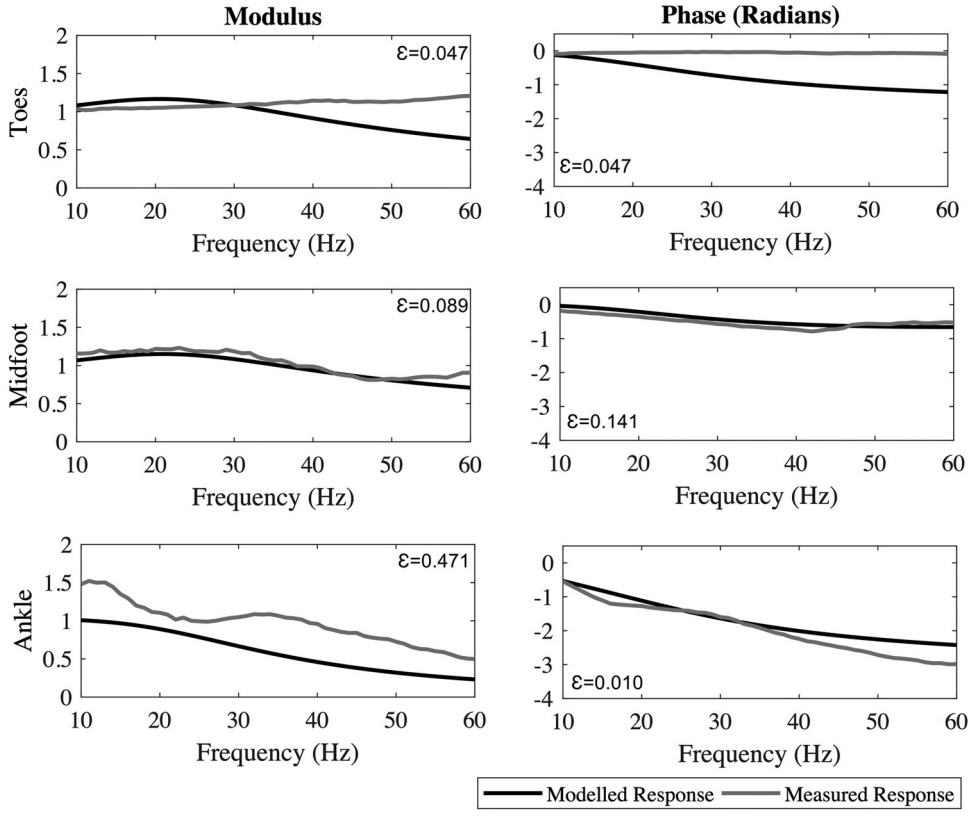


Figure 6. The modelled (black) and measured (grey) transmissibility modulus and phase responses of the ankle, midfoot, and toes of the barefoot in a natural standing position exposed to vertical vibration between 10 and 60 Hz (Goggins et al. 2019a).

and damping of the tarsal fat pad $(k_4, c_4)$ are opposites, where the stiffness is the greatest in the forward, natural, and backward COP location respectively; the damping is greatest in the backward, natural, and forward COP location, respectively.

The transmissibility and phase angle of the modelled and measured responses of the ankle, midfoot, and toes while in the natural standing position are presented in Figure 6. The mean-squared error ($\varepsilon$) percentage between the measured and modelled transmissibility response was 4.7, 8.9, and 47.1% at the toes, midfoot, and ankle respectively (Table 2). From the proposed model of the FAS, the greatest variance in transmissibility response occurred at the ankle. Whereas, the mean-squared error ($\varepsilon$) percentage between the measured and modelled phase angle response was 4.7, 14.1, and 1.0% at the toes, midfoot, and ankle respectively, with the greatest difference being at the midfoot (Table 2).

Similarly, the transmissibility and phase angle of the modelled and measured responses of the ankle, midfoot, and toes while in the standing forward COP position are presented in Figure 7. The mean-squared error ($\varepsilon$) percentage with the COP forward towards the toes, was 5.7, 5.8, and 53.9% at the toes, midfoot, and ankle respectively with the greatest difference

occurring at the ankle (Table 2). Whereas, the mean-squared error ($\varepsilon$) percentage between the phase angle responses were 8.1% (toes), 27.5% (midfoot), and 15.4% (ankle).

Of the three modelled COP positions, the backward COP had the poorest response at the ankle ($\varepsilon = 109\%$) (Figure 8). The mean-squared error between the modelled and measured transmissibility responses is much smaller ($\varepsilon = 21.9$ and 3.9%) at the midfoot and toes, respectively (Table 2). The mean-squared error ($\varepsilon$) percentage for the phase angle response were 8.1% (toes), 10.9% (midfoot), and 117% (ankle), again where the response at the ankle was modelled the poorest.

**Table 2.** Mean-squared error ($\varepsilon$) between the reference function and optimised modelled response of the three segment, four degrees-of-freedom lumped parameter model of the foot-ankle system.

| | Modulus | | | Phase (radians) | | |
|---|---|---|---|---|---|---|
| | Forward | Natural | Backward | Forward | Natural | Backward |
| Toes | 0.057 | 0.047 | 0.039 | 0.081 | 0.047 | 0.081 |
| Midfoot | 0.058 | 0.089 | 0.219 | 0.275 | 0.141 | 0.109 |
| Ankle | 0.539 | 0.471 | 1.09 | 0.154 | 0.010 | 1.174 |

### 3.1. Sensitivity analysis

Results of the Monte Carlo sensitivity analysis are presented for the four-DOF LP model of the FAS in the natural (Figure 9), forward (Figure 10), and the backward (Figure 11) COP positions. In general, the transmissibility function variability stimulated by the randomised deviation in the stiffness and damping coefficients (black lines) was always smaller than the measured variability of the participants (grey area) (Goggins et al. 2019a, 2019b).

The variability (as a percentage) between the optimised functions and the Monte Carlo simulated functions are presented for the transmissibility (Figure 12) and phase (Figure 13) at 10 Hz intervals. Overall, the variability was lower for the transmissibility ($10.1 \pm 6.2\%$) than the phase ($22.0 \pm 14.9\%$). As anticipated for the transmissibility sensitivity variance analysis, the variance was the highest at the ankle regardless of COP location. The ankle appeared to become less sensitive as the transmissibility increased, whereas the midfoot and toes became more sensitive as the transmissibility increased. Although, the phase sensitivity variance analysis revealed the midfoot had the highest variance

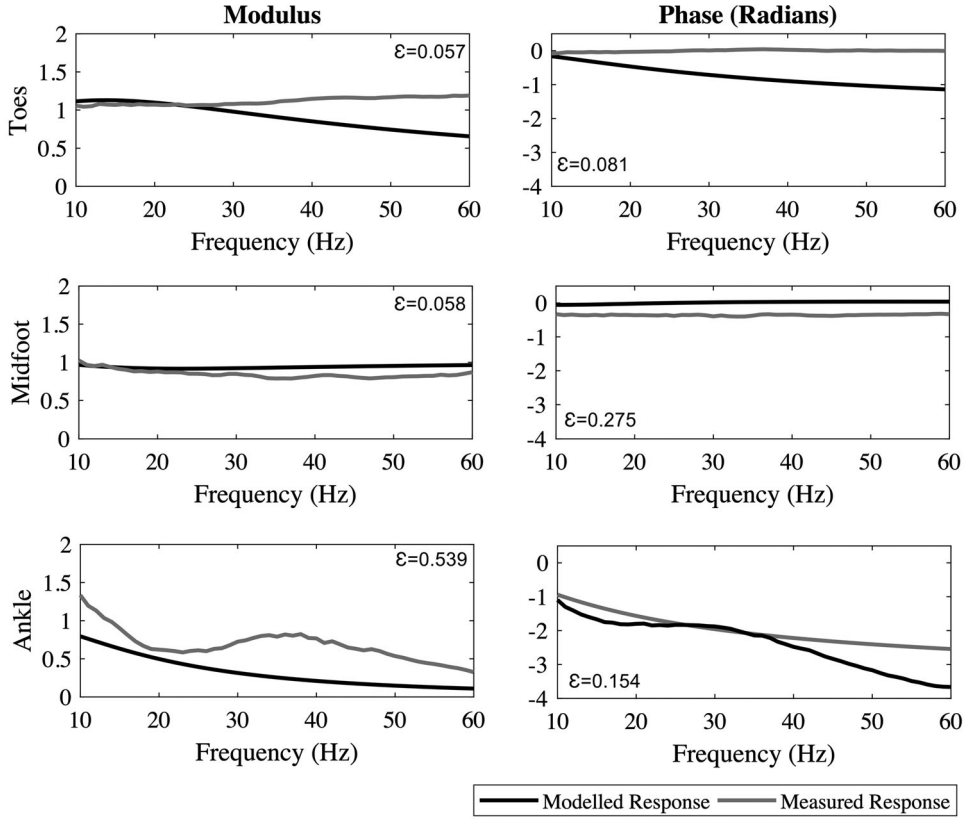


**Figure 7.** The modelled (black) and measured (grey) transmissibility modulus and phase responses of the ankle, midfoot, and toes of the barefoot standing with the COP towards the forefoot, while exposed to vertical vibration between 10 and 60 Hz (Goggins et al. 2019b).

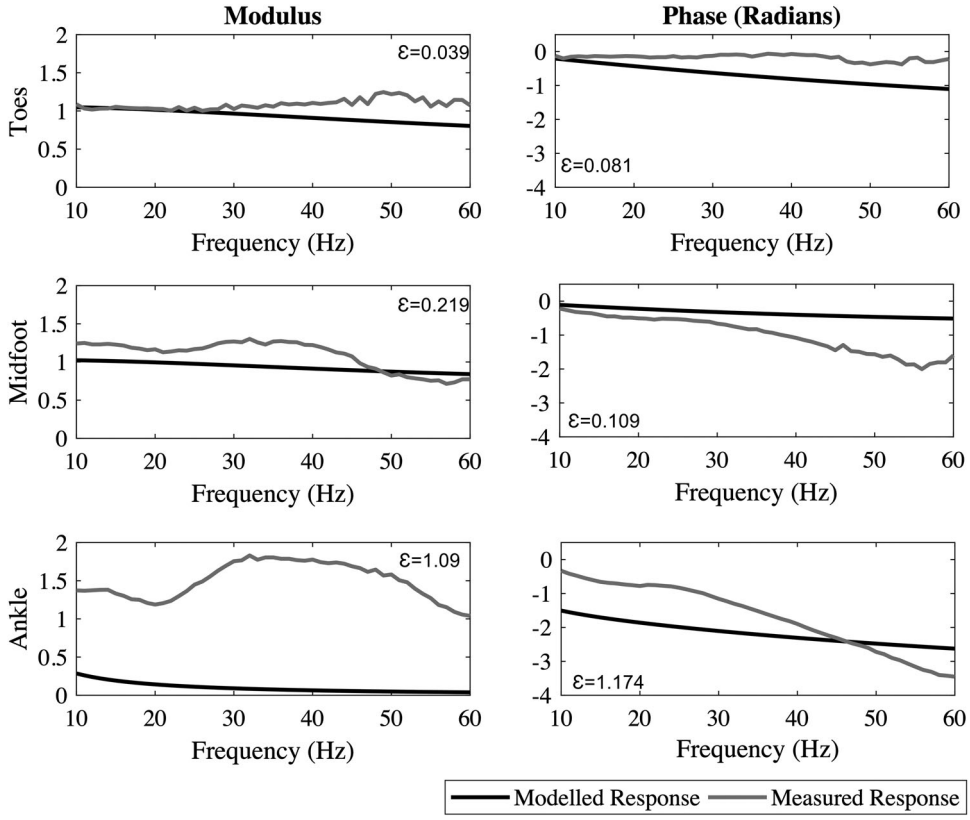


Figure 8. The modelled (black) and measured (grey) transmissibility modulus and phase responses of the ankle, midfoot, and toes of the barefoot standing with the COP towards the rearfoot, while exposed to vertical vibration between 10 and 60 Hz (Goggins et al. 2019b).

regardless of COP location, and there was not a visible trend in sensitivity depending on the frequency.

## 4. Discussion

The purpose of this paper was to develop a simple model of the FAS system and to determine whether such a model could predict the experimental vibration response in each of the three COP scenarios. The K-means analysis of previously published data (Goggins et al. 2019a, 2019b) suggested that three measurement locations would be sufficient for modelling the transmissibility response of the FAS: the nail of the big toe (T1P1), the third metatarsal (L2), and the lateral malleolus (L4). Using the truss-structure framework from Simkin and Leichter (1990) and Kim and Voloshin (1995), a three-segment, 4-DOF LP model of the FAS exposed to vertical vibration from 10 to 60 Hz was created. The model was then fit to the transmissibility measurements from 21 participants (Goggins et al. 2019a) in order to assess the effects of changing the COP location on the model parameters (Goggins et al. 2019b).

A different set of optimal anatomical measurement locations were identified in a previously published study (Goggins et al. 2020) via multiple correspondence analysis of the transmissibility magnitudes. The current work used a different analytical approach to capture the transmissibility frequency differences – clustered K-means analysis of the transmissibility response curves – to arrive at a comparable set of measurement locations. The former analysis suggests four sites (T1P1, T1P3, M1, and L4) are needed to characterise transmissibility magnitude differences in the biodynamic response of the foot to FTV, while the later suggest three (T1P1, L2, and L4) for the transmissibility frequency curves. The relative agreement between the two methods is noteworthy given the different analyses by which and different experimental features from which, they were obtained. Though there are differences in the specific locations recommended, both approaches separate locations at the ankle, midfoot, and toes, with the T1P3 location being grouped in with the midfoot (Figure 2).

Based on the recommended three measurement locations, a simplified model of the foot was developed which included the medial longitudinal arch and

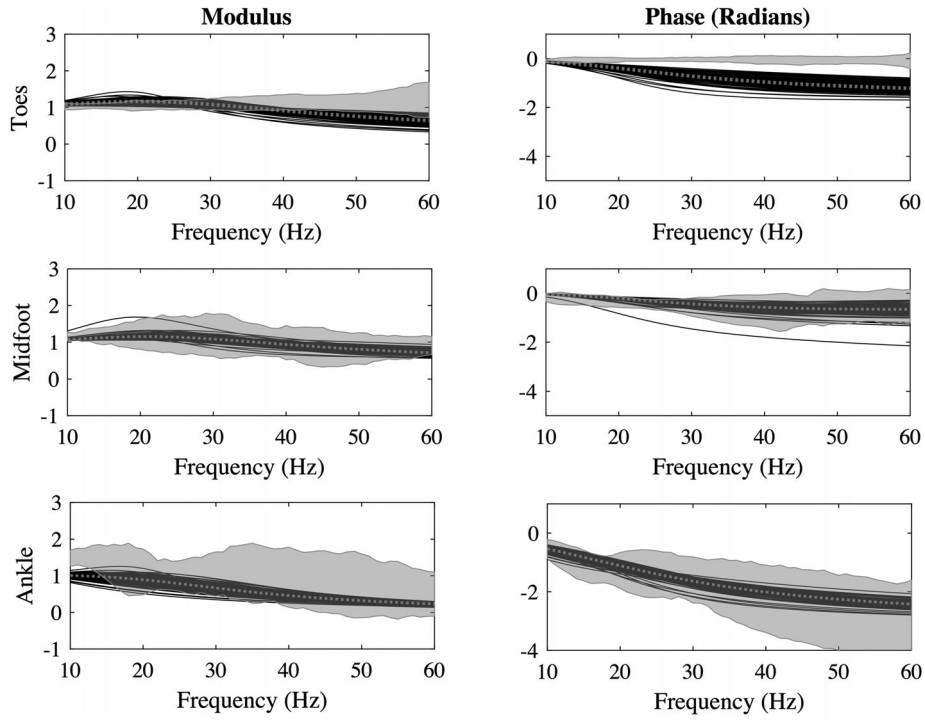


Figure 9. Model sensitivity (black curve) for the natural COP position (grey dotted line) and measured ± standard deviation (grey area) (Goggins et al. 2019a) of the transmissibility modulus and phase computed at three modelled locations (toes, mid-foot, ankle).

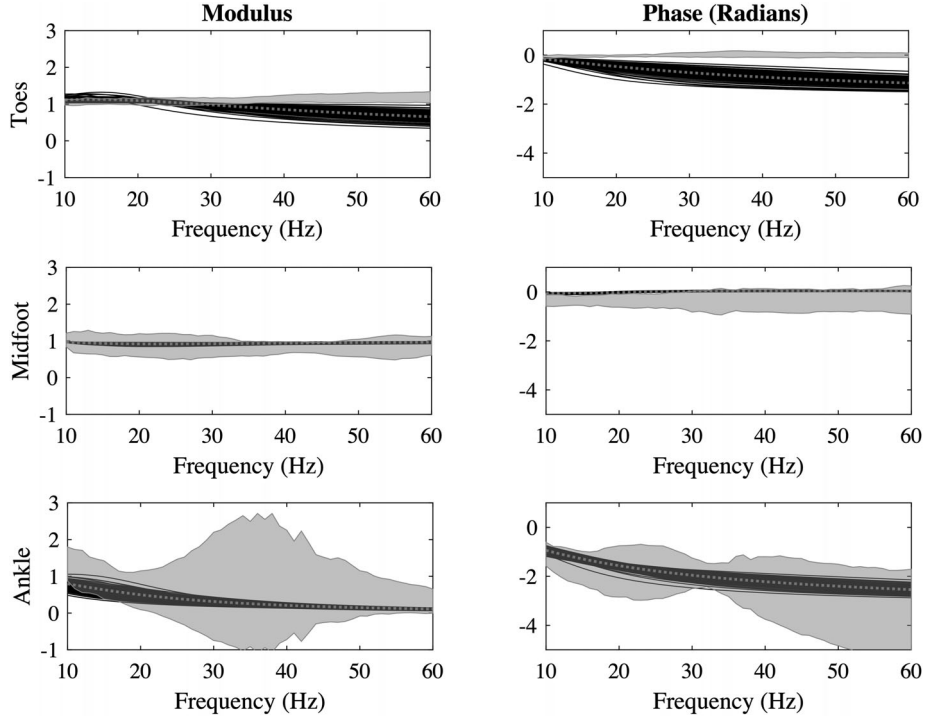


Figure 10. Model sensitivity (black curve) for the forward COP position (grey dotted line) and measured ± standard deviation (grey area) (Goggins et al. 2019b) of the transmissibility modulus and phase computed at three modelled locations (toes, mid-foot, ankle).

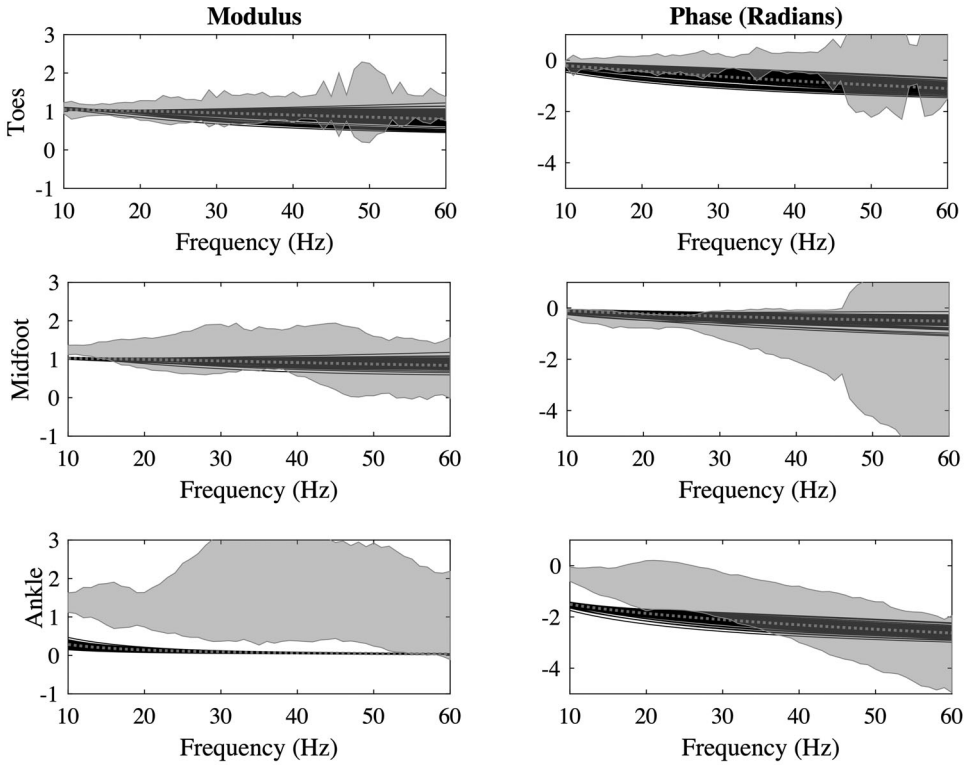


Figure 11. Model sensitivity (black curve) for the backward COP position (grey dotted line) and measured ± standard deviation (grey area) (Goggins et al. 2019b) of the transmissibility modulus and phase computed at three modelled locations (toes, midfoot, ankle).

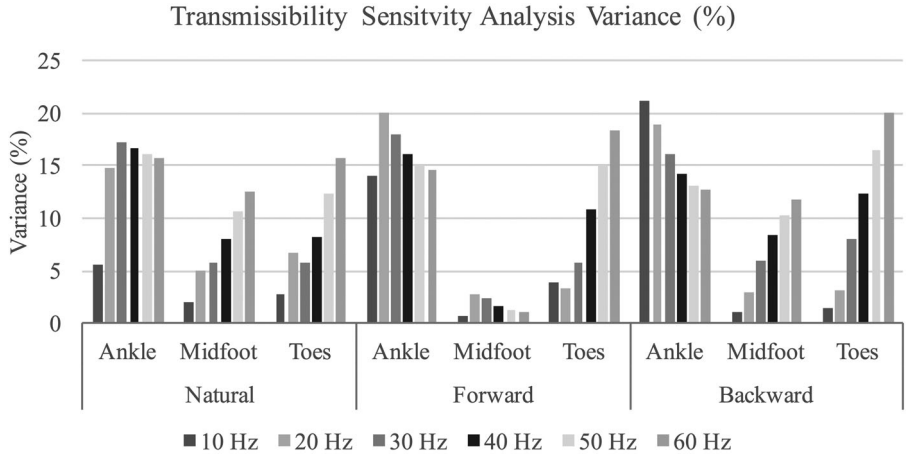


Figure 12. The percentage of deviation between the optimised transmissibility function and the Monte Carlo simulated transmissibility functions, in three COP locations (natural, forward, backward) at 10 Hz intervals.

the plantar aponeurosis. These two features were incorporated in the model because of previous studies that highlight their importance to the biomechanics of the foot in gait. Interestingly, the large stiffness ($41.1 \times 10^4$–$286.2 \times 10^4$ N/m) and negligible damping (0.1 Ns/m) values of the spring-damper system representing the plantar aponeurosis suggest that it does not play a significant role in vibration absorption. Similar results were found by Kim and Voloshin (1995) when the foot was modelled with and without a plantar fascia; the absence of the fascia only caused a 10% change in the impact acceleration of the ankle joint, implying an insignificant role in shock absorption. However, the difference in the current study between the stiffness in the forward ($133.2 \times 10^4$ N/m) and backward ($41.1 \times 10^4$ N/m) COP locations may be explained by the increased tension of the plantar aponeurosis (Salathe, Arangio, and Salathe 1986).

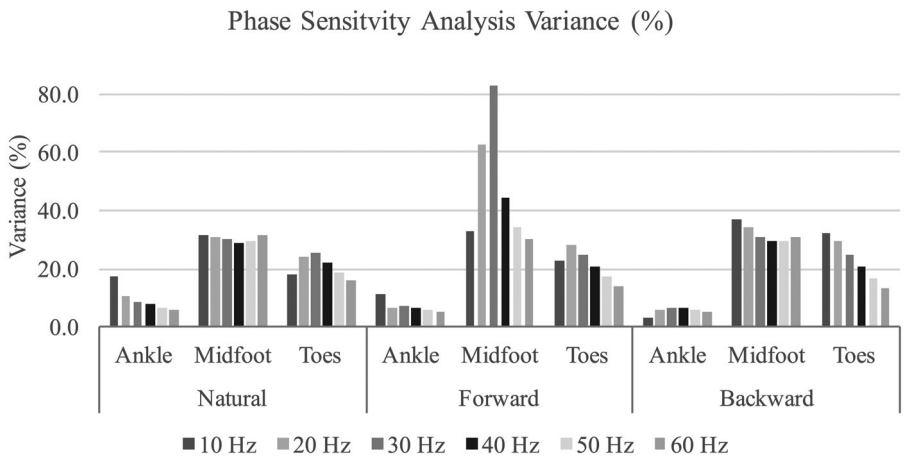


Figure 13. The percentage of deviation between the optimised phase function and the Monte Carlo simulated phase functions, in three COP locations (natural, forward, backward) at 10 Hz intervals.

Concentrating the pressure towards the toes could cause a flattening of the arch as the pressure underneath the heel is being released.

Other important changes were observed as a function of COP. The spring-dampers beneath the tarsal heads and calcaneus, the two contact points between the foot and the platform (Salathe, Arangio, and Salathe 1986), exhibited the largest changes based on COP. When the COP location is pushed forward towards the toes, the stiffness at the tarsal fat pad increased from $64.6 \times 10^3$ N/m (natural) to $55.6 \times 10^4$ N/m and the damping decreased from $7.88 \times 10^3$ Ns/m (natural) to the model minimum of 0.10 Ns/m. Conversely, when the COP location shifts backward towards the heel, the stiffness at the tarsal fat pad is diminished to 102 N/m and the damping increases substantially ($25.2 \times 10^4$ Ns/m). The nature of the observed changes suggests that increased loading on the soft tissues increases their stiffness and damping response. The reverse trend was observed in the calcaneus fat pad, with stiffness increasing and damping decreasing (Fontanella et al. 2016) as the COP was shifted towards the rearfoot.

Simplifying assumptions are unavoidable when trying to build a computationally efficient model of a complex system (Morales-Orcajo, Bayod, and Barbosa de Las Casas 2016). For example, the model presented in this paper is limited to three segments and only vertical axis vibration in order to limit the number of experimental measurement locations needed on the foot. It has also constrained the frequency range to 10–60 Hz as these values are most representative of the FTV exposure seen in industry (Eger et al. 2014). This model is also limited by the experimental data, which lumps together people of different ages, sex, anthropometry, arch height, etc. All these factors are expected to alter the response of the foot to FTV; however, the exact nature of these relationships has not been identified experimentally. Future work must not only establish the significance of these parameters but also evaluate the value of incorporating them into predictive LP models.

One of the goals of this work was to evaluate the efficacy of a simple model of the foot at predicting the responses to FTV. Increasing model complexity needs to be evaluated cautiously. More segments may be added to the model to increase its predictive powers; however, each change represents increased costs in terms of both computational needs and the experimental data necessary to validate such a model. These costs may appear minor when considering the foot in isolation, but become more burdensome when combined with other regions (e.g. lower limbs, trunk, head) to investigate WBV. Therefore, the clinical value of the predictions must guide the development to ensure an 'improved' model provides useful insights into the risk of VWT. The effects of vibration in multiple axes (*x*, *z*, and potentially the rotational axes) could be evaluated and modelled. Future work should also consider the effects of raising the heel above the plane of the metatarsals (Dawe and Davis 2011) to evaluate and reproduce the effects of insoles and footwear. The incorporation of these structures would allow designers to investigate what height, stiffness and damping characteristics of the insole and boot are most effective at reducing FTV exposure.

## 5. Conclusions

The three-segment, 4-DOF LP model of the FAS exposed to vertical vibration from 10 to 60 Hz presented herein provides reasonable results at the ankle,

midfoot, and toes in the natural standing position ($\varepsilon = 0.471$, 0.089, and 0.047) and with the COP pushed forward towards the toes ($\varepsilon = 0.539$, 0.058, and 0.057). However, when the COP is pushed backward towards the hindfoot, the model does not sufficiently capture the transmissibility response at the ankle ($\varepsilon = 1.09$, 0.219, and 0.039). While the current work represents a useful initial model of the vibration response of the foot, further refinements are needed to fully capture its behaviour under a variety of loading scenarios.

## Disclosure statement

No potential conflict of interest was reported by the author(s).

## Funding

This work was supported by a Natural Science and Engineering Council of Canada Discovery Grant [RGPIN/4252-2015].

## ORCID

Tammy Eger http://orcid.org/0000-0003-3830-0773

## References

Aruin, A. S., and V. M. Zatsiorsky. 1984. "Biomechanical Characteristics of Human Ankle-Joint Muscles." *European Journal of Applied Physiology and Occupational Physiology* 52 (4): 400–406. (doi:10.1007/BF00943370.

Chadefaux, D., K. Goggins, C. Cazzaniga, P. Marzaroli, S. Marelli, R. Katz, T. Eger, and M. Tarabini. 2020. "Development of a Two-Dimensional Dynamic Model of the Foot-Ankle System Exposed to Vibration." *Journal of Biomechanics* 99 (23): 109547–109512. doi:10.1016/j.jbiomech.2019.109547.

Coermann, R. R. 1962. "The Mechanical Impedance of the Human Body in Sitting and Standing Position at Low Frequencies." *Human Factors* 4: 227–253. doi:10.1177/001872086200400502.

Dawe, E. J. C., and J. Davis. 2011. "(vi) Anatomy and Biomechanics of the Foot and Ankle." *Orthopaedics and Trauma* 25 (4): 279–286. doi:10.1016/j.mporth.2011.02.004.

Dong, Jennie H., Ren G. Dong, Subhash Rakheja, Daniel E. Welcome, Thomas W. McDowell, and John Z. Wu. 2008. "A Method for Analyzing Absorbed Power Distribution in the Hand and Arm Substructures When Operating Vibrating Tools." *Journal of Sound and Vibration* 311 (3–5): 1286–1304. doi:10.1016/j.jsv.2007.10.031.

Dong, Ren G., Jennie H. Dong, John Z. Wu, and Subhash Rakheja. 2007. "Modeling of Biodynamic Responses Distributed at the Fingers and the Palm of the Human Hand-Arm System." *Journal of Biomechanics* 40 (10): 2335–2340. doi:10.1016/j.jbiomech.2006.10.031.

Eger, Tammy, Aaron Thompson, Mallorie Leduc, Kristine Krajnak, Katie Goggins, Alison Godwin, and Ron House. 2014. "Vibration Induced White-Feet: Overview and Field Study of Vibration Exposure and Reported Symptoms in Workers." *Work* 47 (1): 101–110. doi:10.3233/WOR-131692.

Fontanella, Chiara Giulia, Federica Nalesso, Emanuele Luigi Carniel, and Arturo N. Natali. 2016. "Biomechanical Behavior of Plantar Fat Pad in Healthy and Degenerative Foot Conditions." *Medical & Biological Engineering & Computing* 54 (4): 653–661. doi:10.1007/s11517-015-1356-x.

Gefen, A. 2003. "The In Vivo Elastic Properties of the Plantar Fascia during the Contact Phase of Walking." *Foot & Ankle International* 24 (3): 238–244. doi:10.1177/107110070302400307.

Goggins, Katie A., Bruce E. Oddson, W. Brent Lievers, and Tammy R. Eger. 2020. "Anatomical Locations for Capturing Magnitude Differences in Foot-Transmitted Vibration Exposure Determined Using Multiple Correspondence Analysis." *Theoretical Issues in Ergonomics Science* 21 (5): 562–576. doi:10.1080/1463922X.2020.1731623.

Goggins, Katie A., Marco Tarabini, W. Brent Lievers, and Tammy R. Eger. 2019a. "Biomechanical Response of the Human Foot When Standing in a Natural Position while exposed to vertical vibration from 10-200 Hz." *Ergonomics* 62 (5): 644–656. doi:10.1080/00140139.2018.1559362.

Goggins, Katie A., Marco Tarabini, W. Brent Lievers, and Tammy R. Eger. 2019b. "Standing Centre of Pressure Alters the Vibration Transmissibility Response of the Foot." *Ergonomics* 62 (9): 1202–1213. doi:10.1080/00140139.2019.1626490.

Gupta, M., and T. C. Gupta. 2017. "Modal Damping Ratio and Optimal Elastic Moduli of Human Body Segments for Anthropometric Vibratory Model of Standing Subjects." *Journal of Biomechanical Engineering* 139 (10): 1–13. doi:10.1115/1.4037403.

Gurram, R., S. Rakheja, and G. J. Gouw. 1995. "Mechanical Impedance of the Human Hand-Arm System Subject to Sinusoidal and Stochastic Excitations." *International Journal of Industrial Ergonomics* 16 (2): 135–145. doi:10.1016/0169-8141(94)00092-H.

Hasiguichi, T., H. Yanagi, Y. Kinugawa, H. Sakakibara, and S. Yamada. 1994. "Pathological Changes of Fingers and Toe in Patients with Vibration Syndrome." *Nagoya Journal of Medical Science* 57: 129–136.

Hedlund, U. 1989. "Raynaud's Phenomenon of Fingers and Toes of Miners Exposed to Local and Whole-Body Vibration and Cold." *International Archives of Occupational and Environmental Health* 61 (7): 457–461. doi:10.1007/BF00386479.

House, R., D. Jiang, A. Thompson, T. Eger, K. Krajnak, J. Sauve, and M. Schweigert. 2011. "Vasospasm in the Feet in Workers Assessed for HAVS." *Occupational Medicine* 61 (2): 115–116. doi:10.1093/occmed/kqq191.

Isman, R. E., and V. T. Inman. 1969. "Anthropometric Studies of the Human Foot and Ankle." *Bulletin of Prosthetics Research* : 97–129.

ISO-2631-1. 1997. *Mechanical Vibration and Shock – Evaluation of Human Exposure to Whole-Body Vibration – Whole-Body Vibration – Part 1: General Requirements*. Geneva, Switzerland: International Organization for Standardization.

Jack, R. J., and M. Oliver. 2008. "A Review of Factors Influencing Whole-Body Vibration Injuries in Mobile Forest Machinery Operators." *International Journal of Forest*

*Engineering* 19 (1): 51–64. doi:10.1080/14942119.2008.10702560.

Ji, T., D. Zhou, and Q. Zhang. 2013. "Models of Standing Human Body in Vertical Vibration." *Proceedings of the Institution of Civil Engineers – Structures and Buildings* 166 (7): 367–378. doi:10.1680/stbu.12.00010.

Kim, W., and A. S. Voloshin. 1995. "Role of Plantar Fascia in the Load Bearing Capacity of the Human Foot." *Journal of Biomechanics* 28 (9): 1025–1033. doi:10.1016/0021-9290(94)00163-X.

Leduc, Mallorie, Tammy Eger, Alison Godwin, James P. Dickey, and Ron House. 2011. "Examination of Vibration Characteristics, and Reported Musculoskeletal Discomfort for Workers Exposed to Vibration via the Feet." *Journal of Low Frequency Noise, Vibration and Active Control* 30 (3): 197–206. doi:10.1260/0263-0923.30.3.197.

MacQueen, J. 1965. "Some Methods for Classification and Analysis of Multivariate Observations." In 5th Berkeley Symposium on Mathematical Statistics and Probability. Berkeley, CA: University of California Press.

Mishoe, J. W., and C. W. Suggs. 1977. "Hand-Arm Vibration Part II: Vibrational Responses of the Human Hand." *Journal of Sound and Vibration* 53 (4): 545–558. doi:10.1016/0022-460X(77)90524-7.

Morales-Orcajo, E., J. Bayod, and E. Barbosa de Las Casas. 2016. "Computational Foot Modeling: Scope and Applications." *Archives of Computational Methods in Engineering* 23 (3): 389–416. doi:10.1007/s11831-015-9146-z.

Reynolds, D. D., and W. Soedel. 1972. "Dynamic Response of the Hand-Arm System to Sinusoidal Input." *Journal of Sound and Vibration* 21 (3): 339–353. doi:10.1016/0022-460X(72)90818-8.

Salathe, E. P., G. A. Jr, Arangio, and E. P. Salathe. 1986. "A Biomechanics Model of the Foot." *Journal of Biomechanics* 19 (12): 989–1001. doi:10.1016/0021-9290(86)90116-8.

Schweigert, M. 2002. "The Relationship between Hand-Arm Vibration and Lower Extremity Clinical Manifestations: A Review of the Literature." *International Archives of Occupational and Environmental Health* 75 (3): 179–185. doi:10.1007/s004200100269.

Simkin, A., and I. Leichter. 1990. "Role of the Calcaneal Inclination in the Energy Storage Capacity of the Human Foot – A Biomechanical Model." *Medical & Biological Engineering & Computing* 28 (2): 149–152. doi:10.1007/BF02441770.

Smith, S. D., and L. E. Kazarian. 1994. "The Effects of Acceleration on the Mechanical Impedance Response of a Primate Model Exposed to Sinusoidal Vibration." *Annals of Biomedical Engineering* 22 (1): 78–87. doi:10.1007/BF02368224.

Subashi, G. H. M. J., Y. Matsumoto, and M. J. Griffin. 2008. "Modelling Resonances of the Standing Body Exposed to Vertical Whole-Body Vibration: Effects of Posture." *Journal of Sound and Vibration* 317 (1-2): 400–418. doi:10.1016/j.jsv.2008.03.019.

Tarabini, Marco, Stefano Solbiati, Giovanni Moschioni, Bortolino Saggin, and Diego Scaccabarozzi. 2014. "Analysis of Non-Linear Response of the Human Body to Vertical Whole-Body Vibration." *Ergonomics* 57 (11): 1711–1723. doi:10.1080/00140139.2014.945494.

Thompson, A. M. S., R. House, K. Krajnak, and T. Eger. 2010. "Vibration-White Foot: A Case Report." *Occupational Medicine* 60 (7): 572–574. doi:10.1093/occmed/kqq107.

Tingsgard, I., and K. Rasmussen. 1994. "Vibration-Induced White Toes." *Ugeskr Laeger* 156 (34): 4836–4838.

Toibana, N., N. Ishikawa, H. Sakakibara, and S. Yamada. 1994. "Raynaud's Phenomenon of Fingers and Toes among Vibration-Exposed Patients." *Nagoya Journal of Medical Science* 57: 121–128.

Wee, B. H. 2012. *The Dynamic Model of the Foot and Ankle System*, 176. Bethlehem, PA: Lehigh University.

Wood, L. A., C. W. Suggs, and C. F. Abrams. 1978. "Hand-Arm Vibration Part III: A Distributed Parameter Dynamic Model of the Human Hand-Arm System." *Journal of Sound and Vibration* 57 (2): 157–169. doi:10.1016/0022-460X(78)90578-3.

Zadpoor, A. A., and A. A. Nikooyan. 2010. "Modeling Muscle Activity to Study the Effects of Footwear on the Impact Forces and Vibrations of the Human Body during Running." *Journal of Biomechanics* 43 (2): 186–193. doi:10.1016/j.jbiomech.2009.09.028.

Zatsiorsky, V. M. 2002. *Kinetics of Human Motion*, 657. Champaign, IL: Human Kinetics.

Zhou, Z., and M. J. Griffin. 2014. "Response of the Seated Human Body to Whole-Body Vertical Vibration: Biodynamic Responses to Sinusoidal and Random Vibration." *Ergonomics* 57 (5): 693–713. doi:10.1080/00140139.2014.898798.